Magnetosome magnetite biomineralization in a flagellated protist: evidence for an early evolutionary origin for magnetoreception in eukaryotes

Pedro Leão,[1] Lucas Le Nagard,[2] Hao Yuan,[2] Jefferson Cypriano,[1] Inácio Da Silva-Neto,[3] Dennis A. Bazylinski,[4] Daniel Acosta-Avalos,[5] Henrique L. de Barros,[5] Adam P. Hitchcock,[2] Ulysses Lins[1] and Fernanda Abreu [ID][1]*

[1]*Instituto de Microbiologia Paulo de Góes, Universidade Federal do Rio de Janeiro, Rio de Janeiro, Brazil.*

[2]*Department of Chemistry & Chemical Biology, McMaster University, Hamilton, ON, Canada.*

[3]*Instituto de Biologia, Universidade Federal do Rio de Janeiro, Rio de Janeiro, Brazil.*

[4]*School of Life Sciences, University of Nevada at Las Vegas, Las Vegas, NV, USA.*

[5]*Centro Brasileiro de Pesquisas Físicas, Rio de Janeiro, Brazil.*

Summary

The most well-recognized magnetoreception behaviour is that of the magnetotactic bacteria (MTB), which synthesize membrane-bounded magnetic nanocrystals called magnetosomes via a biologically controlled process. The magnetic minerals identified in prokaryotic magnetosomes are magnetite (Fe_3O_4) and greigite (Fe_3S_4). Magnetosome crystals, regardless of composition, have consistent, species-specific morphologies and single-domain size range. Because of these features, magnetosome magnetite crystals possess specific properties in comparison to abiotic, chemically synthesized magnetite. Despite numerous discoveries regarding MTB phylogeny over the last decades, this diversity is still considered underestimated. Characterization of magnetotactic microorganisms is important as it might provide insights into the origin and establishment of magnetoreception in general, including eukaryotes. Here, we describe the magnetotactic behaviour and characterize the magnetosomes from a flagellated protist using culture-independent methods. Results strongly suggest that, unlike previously described magnetotactic protists, this flagellate is capable of biomineralizing its own anisotropic magnetite magnetosomes, which are aligned in complex aggregations of multiple chains within the cell. This organism has a similar response to magnetic field inversions as MTB. Therefore, this eukaryotic species might represent an early origin of magnetoreception based on magnetite biomineralization. It should add to the definition of parameters and criteria to classify biogenic magnetite in the fossil record.

Introduction

Magnetotactic bacteria (MTB) are recognized as the simplest organisms that display geomagnetic field orientation, apparently using it to increase the efficiency of chemotaxis in locating and maintaining an optimal position where both electron donors and acceptors are available to the cells (Zhang *et al*., 2010). These bacteria biomineralize intracellular, membrane-bounded, nano-sized crystals of magnetite (Fe_3O_4) or greigite (Fe_3S_4) called magnetosomes via a genetically controlled process. Magnetosomes are generally arranged as a chain within the cell. The chains form a strong enough magnetic dipole to cause the cell to passively align and swim along the Earth's magnetic field lines, a process called magnetotaxis (Bazylinski and Frankel, 2004). Once aligned along the geomagnetic field lines, which are inclined in most regions, magnetotaxis is thought to be advantageous to MTB, in that they will more efficiently locate and maintain an optimal position in vertical chemical and redox gradients in stratified water columns and sediments by reducing a three-dimensional search problem to one of a single dimension (Frankel *et al*., 1997).

Phylogenetically, MTB are extremely diverse. Representatives of this group are present in a number of phyla including several classes of the *Proteobacteria* (Sakaguchi *et al*., 2002; Lefèvre *et al*., 2009; Morillo *et al*., 2014; Taoka *et al*., 2014; Abreu *et al*., 2018), the *Nitrospirae* (Lefèvre *et al*., 2011; Lin *et al*., 2012) and the

candidate phylum *Omnitrophica* (Kolinko *et al*., 2012, 2016). Culture-independent methods and single-cell genome analysis indicate that the diversity and phylogenetic distribution of magnetotactic organisms are underestimated (Kolinko *et al*., 2012; Rinke *et al*., 2013) and may extend to other phylogenetic groups including the phyla *Latescibacteria* and *Planctomycetes* (Lin and Pan, 2015; Lin *et al*., 2017a; Lin *et al*., 2018) or maybe even other domains of life (Torres de Araujo *et al*., 1986).

Studies involving magnetotactic eukaryotic single-celled organisms (e.g., protists) might provide information to potentially fill in gaps regarding the evolution of magnetoreception, that is, between what we know about magnetic-particle-based magnetotaxis in bacteria and what we know about magnetoreception in higher animals, such as bees, fishes or birds (Mann *et al*., 1988; Walker *et al*., 1997; Hanzlik *et al*., 2000; Williams and Wild, 2001; Desoil *et al*., 2005; Johnsen and Lohmann, 2005; Mouritsen, 2018). Thus, it seems logical to examine magnetotaxis/magnetoreception in the protozoa, some of which have been found to magnetically respond to magnetic fields (Bazylinski *et al*., 2000) although not quite as efficiently as cells of MTB. Several types of magnetotactic protists were found and described from a chemically stratified coastal salt pond in Woods Hole, MA, where MTB were also abundant (Bazylinski *et al*., 2000). These protists contained magnetosome-like structures that did not appear to be organized within the cell. In one type, they appeared to be in vacuoles and were extruded from the cell without apparent harm, although no longer displaying magnetotaxis. Further analysis of those magnetic protists revealed that magnetosome-like structures found inside these organisms were identical to those found in MTB present in the same environment (Bazylinski *et al*., 2012), suggesting that the magnetosome-like structures were not biomineralized by the protists but accumulated inside the cells through ingestion of MTB (Monteil *et al*., 2018). Torres de Araujo and colleagues (1986) described a single-celled eukaryotic alga presenting a magnetotactic behaviour more typical of MTB. Unlike the magnetotactic protists described above, cells of this organism contained only anisotropic bullet-shaped magnetite magnetosomes that were clearly organized within the cell as multiple chains traversing the cell along its long axis, suggesting that magnetosome-like structures were biomineralized and organized by the alga itself. Unfortunately, detailed molecular analysis and characterization of this magnetotactic alga were not possible due to the lack of suitable culture-independent techniques at that time.

Recently, Lin and colleagues (2017b) proposed that magnetotaxis in MTB developed during the Archean, suggesting that magnetoreception and the Earth's magnetic field evolved together over time. Understanding the origin and evolution of magnetoreception is clearly important in understanding mechanisms of magnetoreception currently utilized by organisms and possibly to predict future developments in this area, especially in view of the recent unexpected changes in Earth's magnetic field (Witze, 2019). In the present work, we used culture independent techniques to characterize a magnetotactic protist. Our results show that this large magnetotactic, single-celled organism belongs to domain *Eukarya* and that it likely biomineralizes its own unique anisotropic, bullet-shaped, single-magnetic-domain magnetite magnetosomes, which are then organized in the cell as chains. Our results indicate an early origin of a magnetic-particle-based mechanism for geomagnetic field orientation, magnetoreception, by eukaryotes.

Results

Light microscopy observations of magnetically enriched samples from two different rivers, Ururai and Ubatiba, in Rio de Janeiro state (Brazil) revealed the presence of numerous magnetotactic cocci and large magnetotactic microorganisms with a size, structure and motility consistent with a protist (Fig. 1A–C; Supporting Information Video S1). Image analysis showed that these larger cells from both sampling sites were elongated in shape [23.0 $\pm$ 3.3 μm $\times$ 12.5 $\pm$ 2.5 μm (length $\times$ width; $n = 36$)]. These apparent protists contained dark, round intracellular granules at one end of the cell and up to six long, also dark structures that resembled magnetosome chains (arrows; Fig. 1A–C). Flagella were also clearly present on one end of the cell where the dark round granules were concentrated (Fig. 1A and D, arrowheads). This end of the cell appeared to correspond to the anterior portion of the microorganism, that is, the end of the cell that moves forward during swimming, especially taking into consideration the alignment and swimming trajectory of cells along an applied magnetic field (see Supporting Information Video S1).

The response of the putative protist to a sudden reversal of the externally applied magnetic field was very similar to the well-characterized U-turns performed by MTB in the same conditions (see Supporting Information Video S1; Esquivel and Lins de Barros, 1986). The magnetic moment determined using U-turn analysis was $2.5 \pm 1.2 \times 10^{-13}$ A m^2 ($n = 14$), a value about 100 times the magnetic moment of a typical MTB (Frankel and Blakemore, 1980; Esquivel and Lins de Barros, 1986; Wajnberg *et al*., 1986; Petersen *et al*., 1989; Pan *et al*., 2009). The organism exhibited south-seeking polar magnetotaxis, similarly to that of the MTB population in the same sample. The swimming trajectory of this magnetotactic protist displayed a helical nature, while at the same time rotating around its longitudinal axis. This
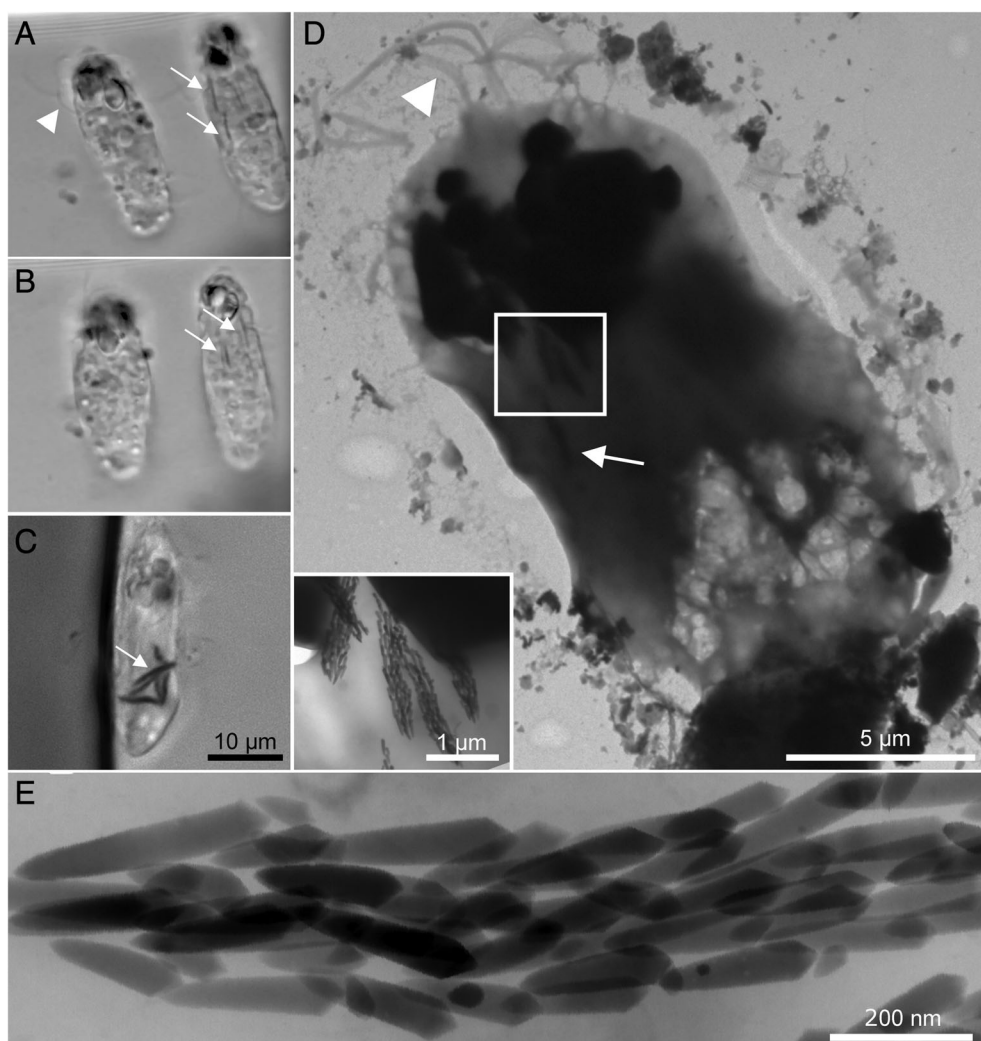
Fig. 1. Light and TEM images of the eukaryotic magnetotactic flagellate described in this study.
A, B. Differential interference contrast microscopy images of the flagellate showing a large intracellular granule at the anterior pole of the cell and long dark filaments close to the cell membrane (arrows) possibly representing magnetosome chains.
C. Phase contrast microscopy image showing globular structures at the cell pole and large dark structures (arrow) possibly corresponding to multiple chains of magnetosomes.
D. TEM of the magnetotactic flagellate confirming the presence of electron dense granules at the anterior region of the cell and a group of flagella emerging from the same end of the cell (arrowhead). The insert represents a high-magnification image of the area delineated by the white square showing several chains of bullet-shape magnetosomes.
E. High-magnification TEM image of the bullet-shaped magnetosomes in a chain localized inside the cell. Scale bar in C applies to A and B.

axis was parallel to the swimming trajectory during the entire swimming motion, and while moving straightforward, cells simultaneously presented a clockwise rotation and a precessional oscillation (Fig. 2; Supporting Information Video S1). The mean cell velocity determined for the magnetotactic protist was 307.5 ± 61.4 μm s^{-1}, with a maximum of 416 μm s^{-1} ($n = 30$). The radius of the helical trajectory was 10.1 ± 3.8 μm and the mean helix angle that is the inclination of the path of the helix (θ) was $15° \pm 6.3°$. The organism presented a mean trajectory angular velocity (ω_t) of 8.1 ± 1.8 rad s^{-1}, a mean body angular velocity (ω_b) of 7.4 ± 1.3 rad s^{-1} and a mean precession angular velocity (ω_p) of 130.3 ± 15.9 rad s^{-1}.

These data from trajectory analysis are displayed in Supporting Information Table SS1.

Transmission electron microscopy (TEM) imaging of the magnetotactic protist confirmed the presence of multiple chains of bullet-shape magnetosomes in the cell (Fig. 1D and E). The number of magnetosomes per chain was about 62 ± 12, formed by three to six subchains (Fig. 1E). Numerous short filamentous structures, presumably flagella, had a mean width of 263.5 ± 30.6 nm ($n = 45$) and were observed at the anterior portion of the organism (Fig. 1D, arrowhead). In total, this organism appears to clearly represent a novel magnetotactic flagellated protozoan.
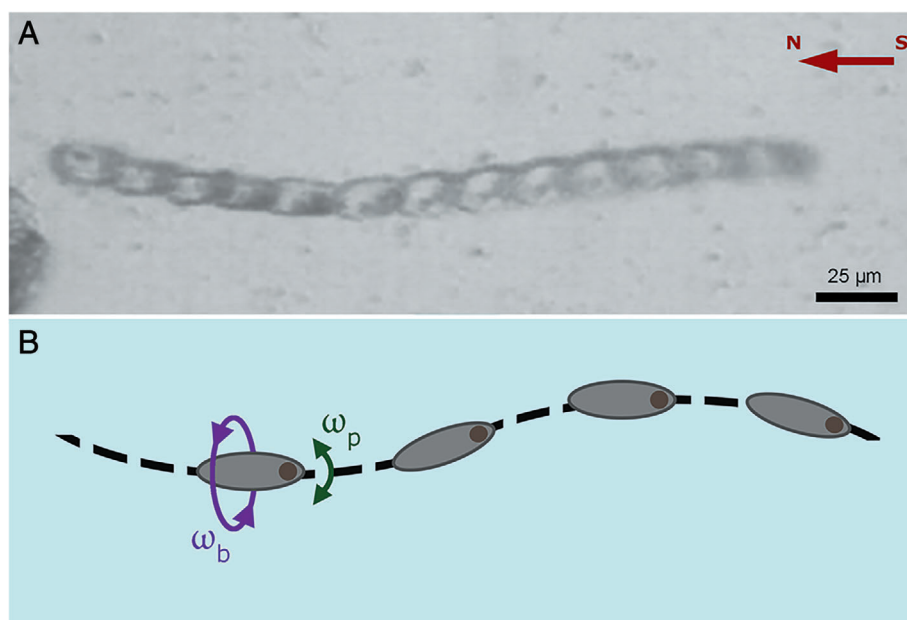
Fig. 2. Swimming motion analysis of the magnetotactic eukaryotic flagellate.
A. Swimming trajectory of the magnetotactic flagellate constructed by joining 13 frames of light microscopy images. The time between adjacent frames is 0.05 s. Note that the trajectory of the microorganism is undulatory as expected for planar projection of a helix. The magnetic field is aligned along the horizontal from right to left (shown by red arrow).
B. Schematic representation of the swimming behaviour of the magnetotactic flagellate showing that, while swimming, the cell rotates around its long axis with angular velocity ω_b (purple arrow) and its long axis oscillates with angular velocity ω_p (blue arrow).

Magnetosomes from MTB found in the same environment as the magnetotactic protist were also anisotropic (bullet shaped) but presented significantly different features (Fig. 3A). Magnetosome crystals from the magnetotactic protist presented 52.7 ± 5.1 nm and 276.6 ± 61.3 nm mean width and length ($n = 201$) respectively. The crystals had sharp edges (Fig. 3B) and a crystal elongation parallel to [100] crystal direction. Magnetosomes from the MTB present in the same environment had more rounded borders and were approximately 42.6 ± 7.6 and 126.2 ± 42.9 nm in width and length, respectively ($n = 263$; Fig. 3C), with a crystal elongation along the [110] direction (Supporting Information Fig. S1).

High-resolution TEM (HRTEM) images and fast Fourier transform (FFT) patterns of the magnetosome crystals in the magnetotactic protist were consistent with magnetite (Fig. 3E). Scanning TEM (STEM; Fig. 3F) and energy dispersive X-ray spectroscopy (EDS) elemental microanalysis of the crystals in the protist showed the presence of iron (Fig. 3G), oxygen (Fig. 3H) and the absence of sulphur (Fig. 3I). FFT patterns of HRTEM and EDS microanalysis of the magnetosomes in MTB were also consistent with magnetite (Supporting Information Fig. S1).

A statistical comparison of length versus width and shape factor distribution between the bullet-shaped magnetosomes of MTB and the protist showed that they are significantly distinct from each other (Fig. 3A and D). When the magnetosome magnetite crystal width was plotted against length, less than 6% of MTB magnetosomes fit in the area where more than 80% of the eukaryotic magnetosome crystals were clustered (Fig. 3A, blue rectangle). Consistent with

this finding, less than 3% of the putative protistan magnetosome crystals fit in the area where 80% of the MTB magnetosome crystals grouped (Fig. 3A, yellow rectangle). A statistical comparison among the size of anisotropic MTB magnetosome crystals previously described in the literature and those described in this work showed that magnetosome crystals observed in the protist under study are very distinct from any bacterial magnetosome crystal (Supporting Information Fig. S2). In addition, the eukaryotic magnetite magnetosome crystals shown here present a mean shape factor of 0.2 ± 0.04 ($n = 201$), whereas bacterial magnetite magnetosome crystals have a mean shape factor of 0.4 ± 0.10 ($n = 263$) with a significant difference between them (p value < 0.0001; Fig. 3D).

A sample of the magnetotactic protist was studied using soft X-ray scanning transmission X-ray microscopy (STXM) with circularly polarized X-rays at the Fe L_{23} edge. This technique enables detection of the X-ray magnetic circular dichroism (XMCD) signal, a measure of the directionality and magnitude of magnetism, which has sensitivity to the different Fe sites in magnetite. Figure 4 presents images and spectra from the STXM–XMCD study. In order to avoid saturation of the X-ray absorption, a smaller chain was studied (green box in Fig. 4A). The bullet-shaped crystals (Fig. 4C) had X-ray absorption spectra consistent with magnetite magnetically ordered either parallel (red in Fig. 4B) or antiparallel (blue in Fig. 4B) to the direction of the spin vector of the X-rays. The sample was tilted by $30°$ to the X-ray propagation axis, which is required to detect in-plane magnetism. When the circular polarization was inverted, the spectral shape of each crystal was changed to the opposite
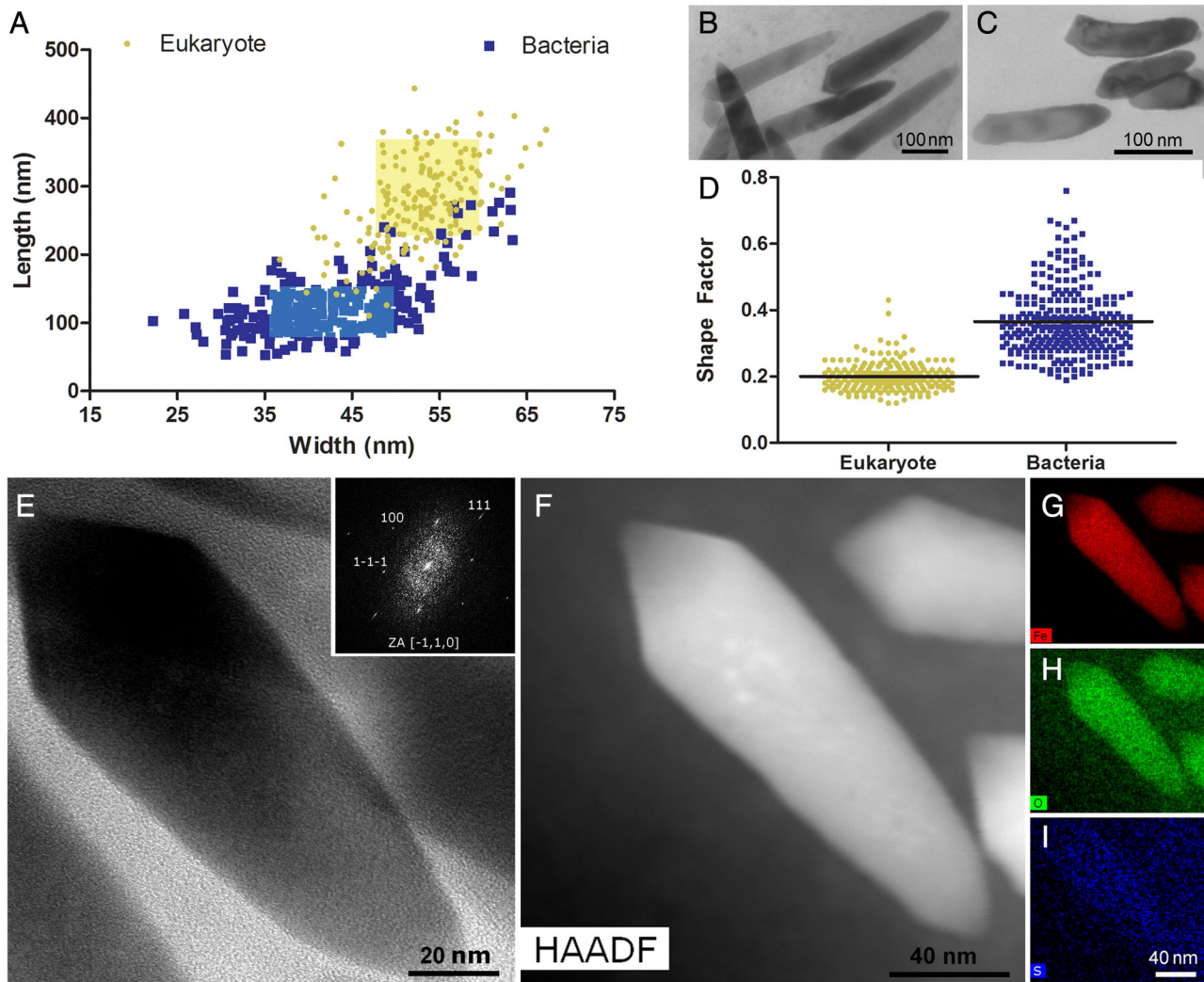
Fig. 3. Comparison of anisotropic magnetite magnetosome crystals from the eukaryotic magnetotactic flagellate with those of MTB present in the same samples.
A. Dot plot showing the relationship between the width and length of anisotropic magnetosomes produced by MTB (blue square) and the eukaryotic flagellate (yellow circle). The blue and yellow rectangles represent the area where 80% of magnetosomes produced by the bacteria and the flagellate fit respectively.
B. TEM image of magnetosomes produced by the magnetotactic flagellate.
C. TEM image of magnetosomes produced by MTB present in the same samples.
D. Dot plot distribution of the shape factor of magnetosomes produced by MTB (blue square) and the flagellate (yellow circle). Black lines represent the mean value for both microorganisms.
E. High-resolution TEM image of an anisotropic magnetite crystal from a magnetosome of the magnetotactic flagellate. Inset shows the fast Fourier transform pattern of the crystal. The pattern is consistent with the mineral magnetite.
F. High-angle annular dark-field image of an isotropic magnetite crystal in a magnetosome of the eukaryotic flagellate.
Correlated elemental maps of (G) iron, (H) oxygen and (I) sulphur of the magnetite crystal shown in (F).

shape. The derived XMCD (antiparallel–parallel; pink curve in Fig. 4C) is generally in agreement with that for magnetite (olive curve in fig. 4C, taken from Goering and colleagues (2007), and scaled to match the height of the positive going XMCD peak at 709.2 eV). However, relative to the XMCD of synthetic magnetite, the overall magnitude is reduced and the third XMCD component at 710.0 eV is very weak, which indicates the site occupancy is quite different from that of stoichiometric magnetite. In particular, the XMCD signal at 710.0 eV in magnetite arises mainly from the Fe(III) octahedral site, which is apparently incompletely filled and non-magnetic in the bullet shaped magnetosomes.

Discussion

Magnetoreception appears to be a common behaviour utilized by many single-celled and multicellular organisms (Mann *et al.*, 1988; Johnsen and Lohmann, 2005; Mouritsen, 2018). Thus far, it has been found in members
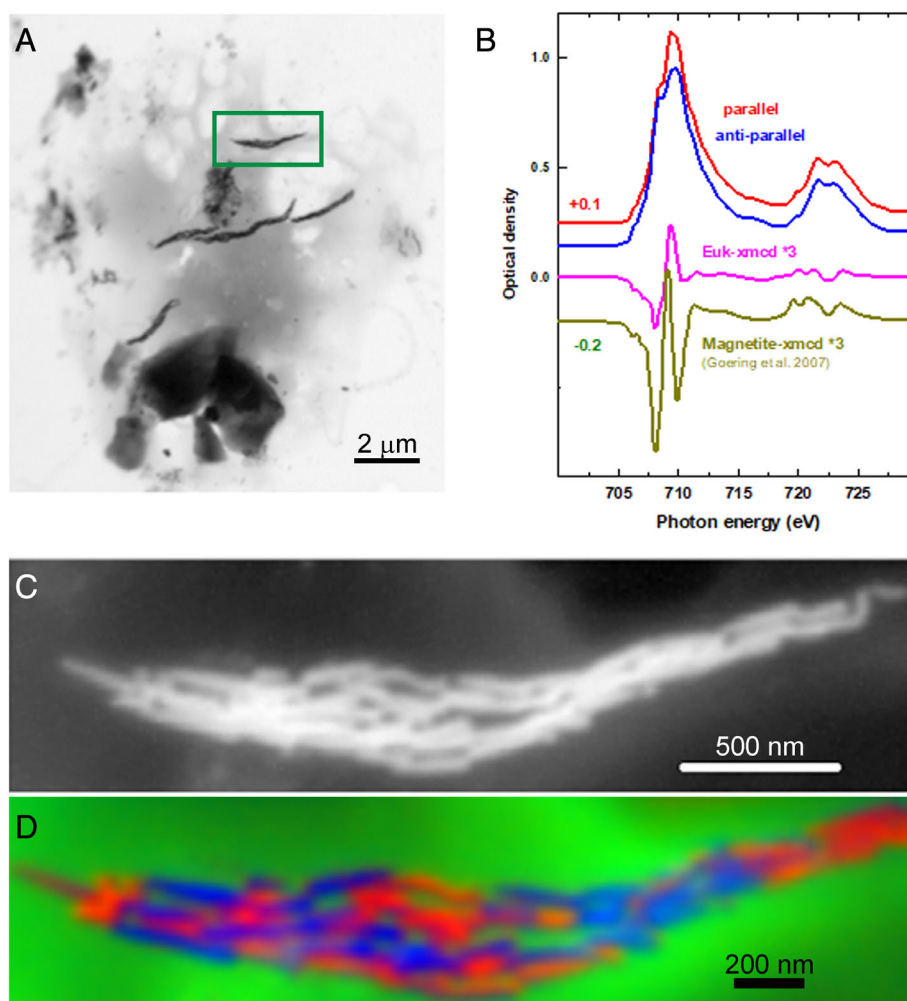
Fig. 4. Spectroscopic investigation of eukaryotic magnetotactic species.
A. Scanning transmission X-ray microscope image at 709.6 eV of cell. The large dark crystals at the bottom are iron oxide particles. The green rectangle indicates the chain of bullet-shaped magnetosomes studied spectroscopically.
B. Fe L_{23} spectra extracted from image sequences measured using circular left (CL) and circular right (CR) polarized X-rays. The red spectrum is that of magnetosomes with shape characteristic of magnetite with its moment oriented parallel (p) to the photon spin vector while that in blue is the antiparallel (a) counterpart. The pink curve, the difference (a − p), is the XMCD signal. The olive curve plotted with an offset is the XMCD signal of synthetic magnetite, normalized so the intensity of the 709 eV signal is the same as that in the protist signal. The two XMCD curves have been multiplied x3 for better visibility.
C. Optical density image of the magnetosome chain in the green box in (A), measured at 709.6 eV.D. Colour-coded composite of component maps of the parallel (red), anti-parallel (blue) and no-Fe (green) signals derived by fitting Fe L_{23} image sequences recorded with CL and CR X-rays.

of the domains *Bacteria* and *Eukarya* but not yet in *Archaea*, although this does not preclude the possibility that it exists in this latter domain. Given the geologic history of Earth and the continual presence of a geomagnetic field on Earth since its creation, life was likely affected by and shaped around changes in the Earth's magnetic field, as it was by other environmental parameters such as the chemistry of the atmosphere and so on. Despite the wide distribution of magnetoreception in organisms on Earth and some suggestions that it is essential for the survival of some of these organisms, elucidation of the various mechanisms of magnetoreception is an emerging field of study. Important questions that have not yet been clearly addressed include: *how did the trait of magnetoreception originate? How did it become distributed to many evolutionarily unrelated organisms? In particular*, if we assume that magnetoreception originated in MTB, which is a reasonable assumption, how did this trait get transferred to eukaryotes?

It was not long after Blakemore (1975) reported on a type of magnetoreception in a diverse group of prokaryotes, the MTB, that a single-celled eukaryote was also found to exhibit magnetoreception in the form of magnetotaxis (Torres de Araujo *et al*., 1986). In this case, a microalga that, like MTB, contained numerous chains of magnetosome-like structures containing crystals of magnetite that imparted a permanent magnetic dipole to the cell (Torres de Araujo *et al*., 1986). This alga was not cultured and was difficult to find and collect and thus little is known about this organism. Later, Bazylinski and colleagues (2000) described a number of diverse magnetotactic protists present in a chemically stratified, coastal salt pond along with MTB. The magnetotactic response of these protists was weaker than MTB and showed a poor directional orientation to external magnetic field lines (Bazylinski *et al*., 2000). Although little detail was provided regarding the putative magnetosomes, similar crystals were also present in the MTB present at the site. In addition, the number of putative magnetosomes was relatively low (explaining the weak magnetotactic response) and, although sometimes present as a chain, did not appear to be organized within the cell. In one type

of protist, they were present as an orange-coloured structure in vacuoles and were extruded from the cell without apparent harm. Interestingly, once extrusion occurred, the protist no longer showed a magnetic response, while the orange structure, still intact, aligned along external magnetic field lines, showing it had a magnetic dipole moment. The authors implied that these protists were grazing on MTB, resulting in their form of magnetotaxis. Here, we describe an eukaryotic flagellate collected from two freshwater rivers in Brazil that displayed a strong magnetotactic behaviour consistent with that found in MTB. Our analyses show that only a single type of magnetosome was found in this eukaryotic microorganism and that they were also unique when compared to those of MTB that possess magnetosomes with a similar morphology. The magnetosome crystals in the flagellate consisted of magnetite and were bullet shaped (anisotropic). Although anisotropic magnetite magnetosomes were also present in some MTB found at the collection site, the magnetosomes in the protist were noticeably different in shape, and particularly in size, from those of magnetosomes in MTB found at the same site, or those of any other MTB described in the literature thus far.

The first question we address is whether the eukaryotic flagellate described here actually displays magnetoreception/magnetotaxis. Thus, we investigated its motility in magnetic fields and compared this to that of MTB. Detailed analysis of helical trajectories in the swimming motion of MTB appears to have only been studied in the many-celled magnetotactic prokaryote (MMP) *Candidatus* Magnetoglobus multicellularis (Almeida *et al*., 2013; Keim *et al*., 2018). Comparing the trajectory parameters of this MMP and the flagellate described here, only θ angle (path inclination in the helical trajectory) measurements were similar among them. Meanwhile, the helical trajectory radius, translational velocity, pitch and trajectory angular velocity from the flagellate were greater than those observed for the MMP. The magnetic moment obtained through U-turn analysis of the magnetotactic flagellate was approximately 20 times greater than the mean magnetic moment measured for the MTB *Ca.* M. multicellularis (Perantoni *et al*., 2009) and *Ca.* Magnetobacterium bavaricum (Mao *et al*., 2014). However, the magnetic moment values determined for the flagellate were similar to those reported for the magnetotactic algae described years ago (Torres de Araujo *et al*., 1986). Flagellates are generally known to be faster swimmers compared to bacteria (McNeill, 1979; Fenchel, 1994), and, accordingly, the swimming speed of the flagellate was greater than that reported for any MTB thus far. The swimming speed of the magnetotactic flagellate was, on average, 35% and 39% greater than that of the magnetotactic cocci *Magnetococcus massalia* strain MO-1 (Lefèvre *et al*., 2009) and *Magnetofaba*

australis strain IT-1 (Morillo *et al*., 2014) respectively. These results show that the magnetotactic flagellate displays a similar magnetotactic response to that of MTB.

The next important question addressed here is whether the magnetotactic flagellate biomineralizes its own magnetosomes. Magnetosomes from some MTB and the flagellate from the same environment were both anisotropic (bullet shaped) but presented significantly different features. Anisotropic magnetosome crystals from the flagellate had sharp edges, a crystal elongation parallel to the [100] crystal direction and were significantly larger than those of the MTB. In addition, those from the MTB had more rounded borders, were smaller than those of the flagellate and were elongated along the [110] direction. The magnetosomes of the flagellate also had a smaller coefficient of variation (CV) determined by length and width measurements (22.2% and 9.7% respectively) than the anisotropic magnetosomes in MTB (34.0% of variation in width and 17.9% in length). It is noteworthy that variation in the width of these magnetosomes was less pronounced than variation in length (Supporting Information Fig. S2). However, the size of the anisotropic magnetite crystals from both the flagellate and the MTB are consistent with being single magnetic domains (Butler and Banerjee, 1975). The smaller CV values of the magnetosomes from the magnetotactic flagellate might suggest a stronger degree of control over the biomineralization of magnetite in the flagellate than in MTB.

Elongated bullet-shaped, anisotropic magnetosomes have been described in MTB phylogenetically affiliated with the *Deltaproteobacteria* subclass of the phylum *Proteobacteria* and the phyla *Omnitrophica* and *Nitrospirae* (Pósfai *et al*., 2013). The elongation axis of magnetosomes in these species varies in the <100>, <110> and <111> crystallographic directions. Those present in the flagellate described here are elongated along [100], the elongation axis described for deep-branching, presumably older, evolutionary groups of MTB (Li *et al*., 2010; Leão *et al*., 2016). In addition, in these deep-branching MTB, the anisotropic magnetosomes are organized as bundles of multiple chains (Li *et al*., 2010; Lefèvre *et al*., 2011). This magnetosome arrangement is also present in the flagellate and thus is not good evidence to distinguish the magnetite magnetosomes biomineralized by the flagellate from those produced by MTB. According to our results, the best parameters to define the eukaryotic origin of magnetite magnetosomes would be crystal length and strict CV values.

Overall, we show that the flagellate described here shows a form of magnetoreception/magnetotaxis very similar, if not the same as in MTB. Moreover, we present strong physical evidence that the putative magnetite magnetosomes in the flagellate are biomineralized by the protozoans themselves. Genetic evidence of magnetite

magnetosome biomineralization, which would consist of finding specific magnetosome genes similar to those in MTB in the genome of the flagellate, would be extremely useful. However, despite numerous attempts to get enough DNA from the flagellate for genome sequencing, we have not yet been successful, most probably due to the difficulty in getting enough cells from the environment for whole genome amplification methods or for isolation of DNA. Determination of the potential magnetosome genes in this flagellate or on any other magnetotactic protist and whether they are related in some way to magnetosome genes in MTB will eventually be essential in determining how magnetoreception/magnetotaxis became established in eukaryotes as well as determining whether or not the genes came from MTB. Results presented here strongly indicate an early origin of magnetoreception in the domain *Eukarya*, a development probably evolving from a protistan ancestor that was able to synthesize magnetic nanoparticles similar to those of MTB from deeply branching phylogenetic groups. Currently, the evolution of magnetotaxis and magnetosome biomineralization in MTB is explained based on vertical and horizontal gene transfer, as well as by gene loss and gene duplication events (Lin *et al*., 2018). Studies of magnetotactic protists would likely provide significant additional information in the evolution of magnetoreception in organisms that respond in some way to the Earth's magnetic field. Recently, Monteil and colleagues (2019) described a mechanism of magnetite-based magnetoreception in a consortium of a non-motile deltaproteobacterium capable of producing magnetite magnetosomes and a flagellated non-magnetotactic protist. The authors suggest that these bacterial and eukaryotic species coevolved resulting in an ancient acquisition of magnetoreception by protist from a deltaproteobacterium that biomineralizes magnetosomes (Monteil *et al*., 2019). Results from further studies involving the ultrastructure and genome sequences of protists displaying magnetotactic behaviour should be important in determining other significant symbiotic events in the evolution of magnetoreception, the development of eukaryotes and of life itself.

This work shows how important it is to continue to look for magnetotactic microorganisms, particularly protozoans, in natural environments. Not only is it important in determining the true phylogenetic diversity of MTB but finding additional magnetotactic protists may prove to be a cornerstone for understanding biomineralization processes and magnetoreception mechanisms in eukaryotes. Finally, a relevant and potentially important aspect of characterizing magnetosomes biomineralized by eukaryotes is in determining their role in the sediment magnetization and in the definition of parameters in the characterization of biogenic magnetite nanoparticles that might be further utilized as magnetofossils in the detection of life or ancient ecosystems based on a stable fossil record.

Experimental procedures

Sampling and magnetic enrichment

Samples of water and sediment were collected in Ubatiba (Maricá, RJ, Brazil; 22°52′49.0″S, 42°48′04.6″W) and Ururaí (Campos dos Goytacazes, RJ, Brazil; 21°45′30.5″S, 41°28′38.4″W) rivers as previously described (Leão *et al*., 2016) during 2015 and 2016. Samples were stored for up to 2 months at room temperature with indirect sunlight. A magnetic enrichment was performed by mixing the sample with a spatula and attaching a magnet on each bottle to attract the magnetotactic microorganisms in the sample. After 20 min, magnetotactic microorganisms were harvested from the magnet area using a micropipette and transferred to 1.5 ml polypropylene tubes. Samples were washed twice with filtered sterilized water from the correspondent sampling site and used for further analysis.

Movement and magnetotactic response analysis

To record the movement of the magnetotactic protist and their response to an applied magnetic field, approximately 100 μl of magnetically enriched sample was observed in an Eclipse TS100 inverted microscope (Nikon, Tokyo, Japan) adapted with a pair of coils attached to the stage. The sample drop was positioned in the middle point between the two coils on the top of a slide. The coil set was able to produce a 5.3 Oe magnetic field in a horizontal direction and to invert the magnetic field orientation by changing the voltage polarity. Movies were recorded at a rate of 82 fps using a digital camera (Infinity 1, Lumenera, Nepean, Canada). Coordinates of 30 protist trajectories were tracked using ImageJ software (NIH) and analyzed using Microcal Origin Software (OriginLab). The parameters calculated were: body angular velocity (ω_b), trajectory angular velocity (ω_t), precession angular velocity (ω_p), translational velocity (V), helical radius (R), helical pitch (P) and helix angle θ between the helix trace and the helix axis (Almeida *et al*., 2013). ω_t was measured from the two-dimensional trajectory projections as shown in Fig. 2. ω_p and ω_b where measured from a frame by frame analysis of the video, following the rotation of the body and the body axis. The U-turn method was used to calculate the protist magnetic moment, as described by De Melo and Acosta-Avalos (2017). Briefly, the magnetic moment direction generated by the pair of coils was inverted to stimulate the movement of the protists, and a new inversion of direction

made the protists to perform U-turn trajectories. The magnetic moment (m) can be estimated using the modified formula described by Esquivel and Lins de Barros (1986):

$$t_u = (A/(mB)) * \ln(2\, mB/kT)$$

where B is the applied magnetic field (5.3 Oe), k is the Boltzmann constant, T is the temperature (approximately 300 K) and A is a constant related to the viscous torque. Considering the protist as a prolate ellipsoid A has the following expression (Stiles and Kagan, 1988):

$$A = (16/3)\pi\eta c^3 / \left[(1/2)\ln((a+c)/(a-c)) - (a*c/b^2) \right]$$

where η is the viscosity of the medium (about 10^{-3} Pa s), a is the ellipsoid major axis, b is the ellipsoid minor axis and $c^2 = a^2 - b^2$.

As the magnetic field is applied in the x direction, during the U-turn, the x coordinate as a function of time must be two straight lines with different slopes. The U-turn time t_u is the time necessary for the change of slope and can be calculated from the derivative dx/dt (De Melo and Acosta-Avalos, 2017). As t_u depends on the constant A, a table of the theoretical values for t_u/A, as a function of m and maintaining η, B and T constant, permits determination of the value of m for each protist via comparison with the experimental values for t_u/A.

Light microscopy

Differential interference contrast (DIC) and phase contrast images were acquired by the observation of approximately 10 µl of magnetically enriched sample using the hanging drop technique (Lefèvre and Bazylinski, 2013) in either a Zeiss AxioPlan or AxioImager D2 microscope (Zeiss, Jena, Germany) equipped with an AxioCam MRC digital camera (Zeiss, Jena, Germany).

Electron microscopy and microanalysis

For direct observation of the magnetotactic protists, whole mount preparations for TEM were made by adding approximately 10 µl of the magnetically enriched sample on top of Formvar-coated copper grids. Conventional TEM images of the protists and MTB were acquired in a Morgagni transmission electron microscope (FEI) operated at 80 kV equipped with a MegaView G2 camera (Olympus, Tokyo, Japan) or in a Tecnai G20 field emission gun microscope (FEI, Hillsboro, OR) operated at 200 kV and equipped with a 4 k × 4 k Gatan UltraScan 1000 CCD camera. For HRTEM, grids were coated with carbon using a Balzers CED030 carbon evaporator

(Bal-Tec, Blazers, Liechtenstein) and observed in a FEG-Titan TEM (FEI Compan, Hillsboro, OR) operated at 300 kV and equipped with a 2 k UltraScan 1000 CCD camera (Gatan, Pleasanton, CA) and four Bruker SDDs detectors (Madison, WI). Fast Fourier transform of HRTEM images were performed by Digital Micrograph software (Gatan, Pleasanton, CA). Energy-dispersive X-ray spectroscopy (EDS) elemental mapping was done using the same microscope in STEM mode to generate elemental maps of oxygen, iron and sulphur.

Magnetosome measurements and statistical analysis

The length, width and shape factor (width/length) of magnetosomes were determined by TEM image analysis using iTEM software (Olympus, Tokyo, Japan). Magnetosome length and width were set as the maximum and minimum inner diameter of each magnetosome respectively. The area corresponding to 80% of the magnetosomes of MTB and magnetotactic protist in Fig. 3A was determined based on the histogram of each dataset. The average (mean) of each dataset was used to set the centre of the most frequent values; groups immediate adjacent to the centre (mean) were added to complete 80% of the total dataset. Statistical analysis of the mean values of shape factors was done by the t-test method. All data analyses were performed using Prism 3.0 software (GraphPad).

Scanning transmission X-ray microscopy and XMCD analysis

Samples were magnetically enriched and a 10 µl droplet was deposited on formvar-coated TEM copper grids and air dried. The same grid which was imaged by TEM was also studied by STXM. The measurements were made using the Research Instruments STXM at the Hermes beamline at the Soleil synchrotron (Swaraj *et al.*, 2017). Measurement and data analysis methods have been described previously (Hitchcock, 2012, 2015). Briefly, images at a specific photon energy and polarization were recorded by detecting the transmitted X-rays in single photon counting mode while (x,y)-raster scanning the sample at the focus of a Fresnel zone plate. Spectra were obtained by collecting image sequences with appropriate range and energy spacing. The transmission images were converted to optical density (OD) using the Io signal measured through formvar off the sample. All data processing was performed using aXis2000 (Hitchcock, 2019). Image sequences in OD representation were fit to reference spectra extracted from representative regions of the area measured, in particular, the off-magnetosome signal which did not exhibit Fe L$_{23}$ signatures, and those of magnetosomes displaying an X-ray

absorption spectral shape like magnetite with either parallel or antiparallel alignment with the X-ray spin vector (Goering *et al.*, 2007). The X-ray circular dichroism spectrum was then derived from the difference of antiparallel and parallel signals.

Acknowledgements

Conflict of interest

The authors declare no conflict of interest.

Author Contributions

P.L. prepared the samples for microscopy analysis and performed TEM and optical microscopy imaging. J.C. performed the HRTEM and EDS analysis. I.D.S.N was responsible for the protozoan classification. D.A.B., U.L. and F.A. were responsible for the experimental design and data analysis. D.A. and H.L.B. were responsible for movement analysis. P.L., F.A. and D.A. were responsible for sampling. A.P.H., L.L.N. and H.Y. performed the STXM measurements and data analysis. P.L., D.A.B. and F.A. wrote the main manuscript text. All of the authors reviewed and contributed to the final manuscript.

References

Abreu, F., Leão, P., Vargas, G., Cypriano, J., Figueiredo, V., Enrich Prast, A., *et al*. (2018) Culture-independent characterization of a novel magnetotactic member affiliated to the Beta class of the Proteobacteria phylum from an acidic lagoon. *Environ Microbiol* **20**: 2615–2624.

Almeida, F.P., Viana, N.B., Lins, U., Farina, M., and Keim, C.N. (2013) Swimming behaviour of the multicellular magnetotactic prokaryote 'Candidatus Magnetoglobus multicellularis' under applied magnetic fields and ultraviolet light. *Antonie Van Leeuwenhoek* **103**: 845–857.

Bazylinski, D.A., and Frankel, R.B. (2004) Magnetosome formation in prokaryotes. *Nat Rev Microbiol* **2**: 217–230.

Bazylinski, D.A., Schlezinger, D.R., Howes, B.H., Frankel, R. B., and Epstein, S.S. (2000) Occurrence and distribution of diverse populations of magnetic protists in a chemically stratified coastal salt pond. *Chem Geol* **169**: 319–328.

Bazylinski, D.A., Lefèvre, C.T., and Frankel, R.B. (2012) Magnetotactic protists at the oxic–anoxic transition zones of coastal aquatic environments. In *Anoxia: Evidence for Eukaryote Survival and Paleontological Strategies*, Altenbach, A.V., Bernhard, J.M., and Seckbach, J. (eds). Dordrecht, the Netherlands: Springer, pp. 131–143.

Blakemore, R. (1975) Magnetotactic bacteria. *Science* **190**: 377–379.

Butler, R.F., and Banerjee, S.K. (1975) Theoretical single-domain grain size range in magnetite and titanomagnetite. *Eur J Vasc Endovasc Surg* **80**: 4049–4058.

De Melo, R.D., and Acosta-Avalos, D. (2017) The swimming polarity of multicellular magnetotactic prokaryotes can change during an isolation process employing magnets: Evidence of a relation between swimming polarity and magnetic moment intensity. *Eur Biophys J* **46**: 533–539.

Desoil, M., Gillis, P., Gossuin, Y., Pankhurst, Q.A., and Hautot, D. (2005) Definitive identification of magnetite nanoparticles in the abdomen of the honeybee *Apis mellifera*. *J Phys* **17**: 45–49.

Esquivel, D.M.S., and Lins de Barros, H.G.P. (1986) Motion of magnetotactic microorganisms. *J Exp Biol* **121**: 153–163.

Fenchel, T. (1994) Motility and chemosensory behaviour of the sulphur bacterium *Thiovulum majus*. *Microbiology* **140**: 3109–3116.

Frankel, R.B., and Blakemore, R.P. (1980) Navigational compass in magnetic bacteria. *J Magn Magn Mater* **15**: 1562–1564.

Frankel, R.B., Bazylinski, D.A., Johnson, M.S., and Taylor, B.L. (1997) Magneto-aerotaxis in marine coccoid bacteria. *Biophys J* **73**: 994–1000.

Goering, E., Lafkioti, M., Gold, S., and Schuetz, G. (2007) Absorption spectroscopy and XMCD at the Verwey transition of Fe_3O_4. *J Magn Magn Mater* **310**: e249–e251.

Hanzlik, M., Heunemann, C., Holtkamp-Rötzler, E., Winklhofer, M., Petersen, N., and Fleissner, G. (2000) Superparamagnetic magnetite in the upper beak tissue of homing pigeons. *Biometals* **13**: 325–331.

Hitchcock, A.P. (2012) Soft X-ray imaging and spectromicroscopy. In *Handbook on Nanoscopy*, Van Tendeloo, G., Van Dyck, D., and Pennycook, S.J. (eds). Hoboken, NJ, USA: Wiley, pp. 745–791.Chapter 22, Volume II.

Hitchcock, A.P. (2015) Soft X-ray spectromicroscopy and ptychography. *J Electron Spectros Relat Phenomena* **200**: 49–63.

Hitchcock, A.P. (2019) *aXis2000 analysis of X-ray images and spectra.* URL http://unicorn.mcmaster.ca/aXis2000.html.

Johnsen, S., and Lohmann, K.J. (2005) The physics and neurobiology of magnetoreception. *Nat Rev Neurosci* **6**: 703–712.

Keim, C.N., de Melo, R.D., Almeida, F.P., Lins de Barros, H.G.P., Farina, M., and Acosta-Avalos, D. (2018) Effect of applied magnetic fields on motility and magnetotaxis in the uncultured magnetotactic multicelular prokaryote 'Candidatus Magnetoglobus multicellularis'. *Environ Microbiol Rep* **10**: 465–474.

Kolinko, S., Jogler, C., Katzmann, E., Wanner, G., Peplies, J., and Schüler, D. (2012) Single-cell analysis reveals a novel uncultivated magnetotactic bacterium within the candidate division OP3. *Environ Microbiol* **14**: 1709–1721.

Kolinko, S., Richter, M., Glockner, F.O., Brachmann, A., and Schüler, D. (2016) Single-cell genomics of uncultivated deep-branching magnetotactic bacteria reveals a conserved set of magnetosome genes. *Environ Microbiol* **18**: 21–37.

Leão, P., Teixeira, L.C., Cypriano, J., Farina, M., Abreu, F., Bazylinski, D.A., *et al*. (2016) North-seeking magnetotactic Gammaproteobacteria in the southern hemisphere. *Appl Environ Microbiol* **82**: 5595–5602.

Lefèvre, C.T., and Bazylinski, D.A. (2013) Ecology, diversity, and evolution of magnetotactic bacteria. *Microbiol Mol Biol Rev* **77**: 497–526.

Lefèvre, C.T., Bernadac, A., Yu-Zhang, K., Pradel, N., and Wu, L.F. (2009) Isolation and characterization of a magnetotactic bacterial culture from the Mediterranean Sea. *Environ Microbiol* **11**: 1646–1657.

Lefèvre, C.T., Pósfai, M., Abreu, F., Lins, U., Frankel, R.B., and Bazylinski, D.A. (2011) Morphological features of elongated-anisotropic magnetosome crystals in MTB of the Nitrospirae phylum and the Deltaproteobacteria class. *Earth Planet Sci Lett* **312**: 194–200.

Li, J., Pan, Y., Liu, Q., Yu-Zhang, K., Menguy, N., Che, R., *et al*. (2010) Biomineralization, crystallography and magnetic properties of bullet-shaped magnetite magnetosomes in giant rod magnetotactic bacteria. *Earth Planet Sci Lett* **293**: 368–376.

Lin, W., and Pan, Y. (2015) A putative greigite-type magnetosome gene cluster from the candidate phylum *Latescibacteria*. *Environ Microbiol Rep* **7**: 237–242.

Lin, W., Li, J., and Pan, Y. (2012) Newly isolated but uncultivated magnetotactic bacterium of the phylum Nitrospirae from Beijing, China. *Appl Environ Microbiol* **78**: 668–675 2012.

Lin, W., Pan, Y., and Bazylinski, D.A. (2017a) Diversity and ecology of and biomineralization by magnetotactic bacteria. *Environ Microbiol Rep* **9**: 345–356.

Lin, W., Paterson, G.A., Zhu, Q., Wang, Y., Kopylova, E., Li, Y., *et al*. (2017b) Origin of microbial biomineralization and magnetotaxis during the Archean. *Proc Natl Acad Sci U S A* **114**: 2171–2176.

Lin, W., Zhang, W., Zhao, X., Roberts, A.P., Paterson, G.A., Bazylinski, D.A., and Pan, Y. (2018) Genomic expansion of MTB reveals an early common origin of magnetotaxis with lineage-specific evolution. *ISME J* **12**: 1508–1519.

McNeill, A.R. (1979) *The Invertebrates*. London, UK: Cambridge University Press.

Mann, S., Sparks, N.H., Walker, M.M., and Kirschvink, J.L. (1988) Ultrastructure, morphology and organization of biogenic magnetite from sockeye salmon, *Oncorhynchus nerka*: Implications for magnetoreception. *J Exp Biol* **140**: 35–49.

Mao, X., Egli, R., Petersen, N., Hanzlik, M., and Zhao, X. (2014) Magnetotaxis and acquisition of detrital remanent magnetization by MTB in natural sediment: First experimental results and theory. *Geochem Geophys Geosyst* **15**: 255–283.

Monteil, C.L., Menguy, N., Prévéral, S., Warren, A., Pignol, D., and Lefèvre, C.T. (2018) Accumulation and

dissolution of magnetite crystals in a magnetically responsive ciliate. *Appl Environ Microbiol* **84**: e02865–e02817.

Monteil, C.L., Vallenet, D., Menguy, N., Benzerara, K., Barbe, V., Fouteau, S., *et al*. (2019) Ectosymbiotic bacteria at the origin of magnetoreception in a marine protist. *Nat Microbiol* **4**: 1088–1095. https://doi.org/10.1038/s41564-019-0432-7.

Morillo, V., Abreu, F., Araujo, A.C., de Almeida, L.G.P., Prast, A.E., Farina, M., *et al*. (2014) Isolation, cultivation and genomic analysis of magnetosome biomineralization genes of a new genus of south-seeking magnetotactic cocci within the Alphaproteobacteria. *Front Microbiol* **5**: 72.

Mouritsen, M. (2018) Long-distance navigation and magnetoreception in migratory animals. *Nature* **558**: 50–59.

Pan, Y., Lin, W., Tian, L., Zhu, R., and Petersen, N. (2009) Combined approaches for characterization of an uncultivated magnetotactic coccus from Lake Miyun near Beijing. *Geomicrobiol J* **26**: 313–320.

Perantoni, M., Esquivel, D.M.S., Wajnberg, E., Acosta-Avalos, D., Cernicchiaro, G., and Lins de Barros, H.G.P. (2009) Magnetic properties of the microorganism *Candidatus* Magnetoglobus multicellularis. *Naturwissenschaften* **96**: 685–690.

Petersen, N., Weiss, D.G., and Vali, H. (1989) Magnetic bacteria in lake sediments. In *Geomagnetism and Paleomagnetism*. Lowes F.J., Collinson D.W., Parry J.H., Runcorn S.K., Tozer D.C., Soward A. (eds). NATO ASI Series (Series C: Mathematical and Physical Sciences). Dordrecht, The Netherlands: Springer, pp. 231–241.

Pósfai, M., Lefèvre, C., Trubitsyn, D., Bazylinski, D.A., and Frankel, R. (2013) Phylogenetic significance of composition and crystal morphology of magnetosome minerals. *Front Microbiol* **4**: 344.

Rinke, C., Schwientek, P., Sczyrba, A., Ivanova, N.N., Anderson, I.J., Cheng, J.F., *et al*. (2013) Insights into the phylogeny and coding potential of microbial dark matter. *Nature* **499**: 431–437.

Sakaguchi, T., Arakaki, A., and Matsunaga, T. (2002) *Desulfovibrio magneticus* sp. nov., a novel sulfate-reducing bacterium that produces intracellular single-domain-sized magnetite particles. *Int J Syst Evol Microbiol* **52**: 215–221.

Stiles, P.J., and Kagan, M. (1988) Frictional torque on an ellipsoid rotating in a uniformly magnetized ferrofluid. *J Colloid Interface Sci* **125**: 493–496.

Swaraj, S., Belkhou, R., Stanescu, S., Rioult, M., Besson, A., and Hitchcock, A.P. (2017) Performance of the HERMES beamline at the carbon K-edge, IOP conference series. *J Phys* **849**: 012046.

Taoka, A., Kondo, J., Oestreicher, Z., and Fukumori, Y. (2014) Characterization of uncultured giant rod-shaped magnetotactic Gammaproteobacteria from a freshwater pond in Kanazawa, Japan. *Microbiol* **160**: 2226–2234.

Torres de Araujo, F.F., Pires, M.A., Frankel, R.B., and Bicudo, C.E.M. (1986) Magnetite and magnetotaxis in algae. *Biophys J* **50**: 375–378.

Wajnberg, E., Salvo de Souza, L.H., Lins de Barros, H.G.P., and Esquivel, D.M.S. (1986) A study of magnetic properties of magnetotactic bacteria. *Biophys J* **50**: 451–455.

Walker, M.M., Diebel, C.E., Haugh, C.V., Pankhurst, P.M., Montgomery, J.C., and Green, C.R. (1997) Structure and function of the vertebrate magnetic sense. *Nature* **390**: 371–376.

Williams, M.N., and Wild, J.M. (2001) Trigeminally innervated iron-containing structures in the beak of homing pigeons, and other birds. *Brain Res* **889**: 243–246.

Witze, A. (2019) Earth's magnetic field is acting up and geologists don't know why. *Nature* **565**: 143–144.

Zhang, W.J., Chen, C., Li, Y., Song, T., and Wu, L.F. (2010) Configuration of redox gradient determines magnetotactic polarity of the marine bacteria MO-1. *Environ Microbiol Rep* **2**: 646–650.

Supporting Information

Additional Supporting Information may be found in the online version of this article at the publisher's web-site:

Figure S1. A) High resolution transmission electron microscopy (HRTEM) image of an anisotropic magnetosome magnetite crystal from a magnetotactic bacterium (MTB) present in the same environment as the magnetotactic flagellates. Inset shows the fast Fourier transform (FFT) pattern of the crystal that is consistent with the mineral magnetite (Fe_3O_4). B) High-angle annular dark-field (HAADF) image of an isotropic magnetite crystal in a magnetosome of the eukaryotic flagellate. Correlated elemental maps of C) oxygen, D) iron, and E) sulfur of the magnetite crystal shown in B).

Figure S2. Comparison of length and width of anisotropic magnetosomes synthesized by magnetotactic bacteria (MTB) and the magnetotactic flagellate. A) Distribution of the mean width by the mean length of the anisotropic magnetosomes in the literature (black cross), in the bacteria isolated from the samples collected in the Ubatiba and Ururai rivers (blue square) and the magnetotactic eukaryotes studied in this work (yellow dot). B) Distribution of the mean length between MTB and the magnetotactic eukaryote. C) Distribution of the mean width between MTB and the magnetotactic eukaryote. Bars corresponding to mean length and width of both microorganisms observed in this study are displayed in blue (bacteria) and yellow (flagellate).

Table S1. Trajectory parameters

Table S2. Comparison between shape and format of anisotropic magnetosome crystals found in magnetotactic microorganisms.

Video S1. Video microscopy of magnetically enriched samples from Ubatiba River showing the magnetotactic response of bacteria and flagellates. Note that both microorganisms perform U-turns upon a sudden reversal of the externally applied magnetic field.